HHS Public Access

Author manuscript

Cell Stem Cell. Author manuscript; available in PMC 2016 April 02.

Published in final edited form as:

Cell Stem Cell. 2015 April 2; 16(4): 400–412. doi:10.1016/j.stem.2015.02.006.

Basal cell carcinoma preferentially arises from stem cells within hair follicle and mechanosensory niches

Shelby C. Peterson[1], **Markus Eberl**[1], **Alicia N. Vagnozzi**[1], **Abdelmadjid Belkadi**[2], **Natalia A. Veniaminova**[1], **Monique E. Verhaegen**[1], **Christopher K. Bichakjian**[1], **Nicole L. Ward**[2], **Andrzej A. Dlugosz**[1], and **Sunny Y. Wong**[1,*]

[1]Departments of Dermatology, and Cell and Developmental Biology, University of Michigan, Ann Arbor, MI 48109, USA

[2]Departments of Dermatology and Neuroscience, Case Western Reserve University, Cleveland, OH 44106, USA

SUMMARY

Basal cell carcinoma (BCC) is characterized by frequent loss of *PTCH1*, leading to constitutive activation of the Hedgehog pathway. Although the requirement for Hedgehog in BCC is well-established, the identity of disease-initiating cells and the compartments in which they reside remain controversial. By using several inducible Cre drivers to delete *Ptch1* in different cell compartments in mice, we show here that multiple hair follicle stem cell populations readily develop BCC-like tumors. In contrast, stem cells within the interfollicular epidermis do not efficiently form tumors. Notably, we observed that innervated *Gli1*-expressing progenitors within mechanosensory touch dome epithelia are highly tumorigenic. Sensory nerves activate Hedgehog signaling in normal touch domes, while denervation attenuates touch dome-derived tumors. Together, our studies identify varying tumor susceptibilities among different stem cell populations in the skin, highlight touch dome epithelia as “hot spots” for tumor formation, and implicate cutaneous nerves as mediators of tumorigenesis.

INTRODUCTION

Dysregulated Hedgehog (Hh) signaling is a hallmark of basal cell carcinoma (BCC), the most common cancer in North America (Epstein, 2008; Kasper et al., 2012). During development and homeostasis, Hh is carefully regulated by a balance of upstream factors that can either promote signaling, such as Smoothened (Smo), or suppress signaling, such as Patched1 (Ptch1). In BCC, this balance is tilted decisively in favor of pathway activation

*correspondence: sunnyw@umich.edu.

AUTHOR CONTRIBUTIONS

SCP and SYW conceived and performed experiments, wrote the manuscript and secured funding. ME, ANV and NAV performed experiments. MEV and CKB provided reagents. AB, NLW and AAD provided expertise and feedback.

through mutations that cause either loss of PTCH1 function or constitutive activation of SMO (Johnson et al., 1996; Xie et al., 1998).

Early evidence implicating perturbed Hh in BCC came from studies which demonstrated that patients harboring a defective *PTCH1* allele are predisposed to developing numerous BCCs (Gorlin's syndrome) (Bonifas et al., 1994; Hahn et al., 1996; Johnson et al., 1996). Similarly, loss of *Ptch1* promotes BCC-like lesions in irradiated mice (Aszterbaum et al., 1999), as does overexpression of mutated forms of Smo, Sonic hedgehog, or downstream Gli transcription factors (Grachtchouk et al., 2000; Mao et al., 2006; Nilsson et al., 2000; Oro and Higgins, 2003; Oro et al., 1997; Xie et al., 1998). Findings from these and other studies have recently culminated in the U.S. Food and Drug Administration's approval of GDC-0449 (vismodegib), an oral inhibitor of SMO, as a therapeutic for treating advanced BCC.

In the skin, multiple stem cell populations maintain tissue homeostasis and contribute to organ regeneration during hair cycling (Jaks et al., 2010). In trying to identify the stem cells which give rise to BCC, however, recent studies have yielded conflicting results (Epstein Jr., 2011). For instance, work by Youssef et al., has suggested that hair follicle bulge stem cells expressing a constitutively active form of Smo (SmoM2) resist BCC formation (Youssef et al., 2010). Rather, these tumors arise primarily from the interfollicular epidermis (IFE), which we have also observed in intact and wounded skin (Wong and Reiter, 2011). In direct contrast, lineage tracing experiments by Wang et al., using irradiated *Ptch1* heterozygous animals have suggested that Keratin 15+ bulge stem cells are the primary progenitors for BCC (Wang et al., 2011). A third possibility—that stem cells in the epidermis and bulge are both competent for tumorigenesis—has also been proposed for tumors induced by an activated form of Gli2 (Grachtchouk et al., 2011).

These discrepant results are likely due to the use of different animal models whereby, in some cases, oncogenic transgenes such as SmoM2 are driven by heterologous promoters. Since up to 90% of human BCCs are thought to be caused by loss of *PTCH1*, mouse models which target deletion of *Ptch1* to specific skin compartments may serve as more accurate models of human disease. Indeed, deletion of *Ptch1* in Lgr5+ stem cells in the lower bulge and secondary hair germ has been reported to yield BCC-like tumors (Kasper et al., 2011). Whether other stem cell populations residing in the hair follicle and IFE possess tumor-forming capacity currently remains unclear.

Here we demonstrate that multiple hair follicle stem cell populations are highly tumorigenic upon deletion of *Ptch1*, while most stem cells within the IFE do not efficiently form tumors. However, an innervated subset of IFE cells known as touch dome epithelia display activated Hh signaling during homeostasis and are highly susceptible to tumorigenesis. Surgical nerve ablation blunted the formation of touch dome-derived lesions, suggesting that cutaneous sensory nerves may play a previously unrecognized role in skin cancer.

RESULTS

BCC-like tumors can arise from multiple hair follicle stem cell populations

A hair follicle origin for BCC has long been suggested based on similarities in marker expression (Jih et al., 1999; Schirren et al., 1997). Since the hair follicle is maintained by several independent stem cell populations, we directly tested whether these cells are able to form tumors upon loss of *Ptch1*. To target *Ptch1* deletion to specific hair follicle compartments, we generated mice harboring homozygous *Ptch1* floxed alleles (Nitzki et al., 2012) coupled with different tamoxifen-inducible Cre drivers (Figure 1A). We treated mice with tamoxifen at 7.5 weeks of age, then harvested skin biopsies several weeks post-induction to assess tumor formation.

During telogen, stem cells expressing the Hh target gene *Gli1* reside within the hair follicle upper and lower bulge and secondary hair germ (Brownell et al., 2011). In mice expressing *Gli1* promoter-driven Cre^{ERT2} and *Ptch1* floxed alleles (*Gli1;Ptch1*), we observed robust tumor formation 5 weeks after tamoxifen induction (Figure 1B). These tumors appeared well-circumscribed and displayed BCC-like features such as peripheral basal palisading (Figure 1C). As expected, these lesions were typically connected to the hair follicle upper and lower bulge, but not the infundibulum, consistent with the lack of contribution of Gli1+ stem cells to the hair canal (Brownell et al., 2011). Although Gli1+ cells can contribute to regenerating hair follicles during anagen, we did not observe tumors associated with the lower anagen follicle, suggesting that matrix cells cannot give rise to BCCs (Figure S1).

We have recently reported that mice expressing *Hes1* promoter-driven Cre^{ERT2} display recombinase activity in suprabasal cells of the IFE and infundibulum (Veniaminova et al., 2013). By coupling this recombinase with an inducible *ROSA26R* promoter-driven *YFP* reporter allele, we also observed Cre activity in inner bulge and, less frequently, in outer bulge stem cells (Figure 1D). We therefore assessed tumor formation in mice expressing this Cre along with *Ptch1* floxed alleles (*Hes1;Ptch1*), and observed upper and lower bulge-associated lesions similar to those in *Gli1;Ptch1* animals, within 7 weeks after tamoxifen induction (Figure 1E). Together, these data confirm that bulge stem cells can indeed serve as tumor progenitors.

To test whether other stem cell populations can form BCCs, we next focused on Lrig1+ cells in the isthmus. Under homeostatic conditions, these cells renew the hair follicle infundibulum independently of bulge stem cells, since bulge cells largely do not contribute to the infundibulum, while Lrig1+ stem cells do not contribute to the bulge or anagen follicle (Page et al., 2013; Veniaminova et al., 2013). In mice expressing *Lrig1* promoter-driven Cre^{ERT2} and *Ptch1* floxed alleles (*Lrig1;Ptch1*), we observed numerous tumors associated with the isthmus and infundibulum 5 weeks after tamoxifen induction (Figure 1F). These findings therefore reveal that BCC-like tumors can originate from upper bulge, lower bulge and isthmus progenitor populations in the hair follicle.

The interfollicular epidermis displays reduced tumor forming capacity

To determine whether the epidermis is susceptible to tumorigenesis, we deleted *Ptch1* in the IFE using mice expressing *Keratin 14* promoter-driven Cre^{ERT} (*K14;Ptch1*). We and others

have previously shown that this recombinase displays robust activity in the IFE, but minimal activity in the hair follicle (Wong and Reiter, 2011; Zhang et al., 2009), as confirmed here using the YFP reporter allele (Figure 2A). Surprisingly, *K14;Ptch1* mice did not develop tumors in the epidermis 5 weeks after induction. Even after extending the interval between tamoxifen treatment and biopsy to 12 weeks, we noticed that *K14;Ptch1* animals typically possessed a hyperplastic epidermis containing small, ectopic hair follicle-like buds resembling early benign follicular hamartomas (Figure 2B). Larger lesions adjacent to the IFE radiated laterally from the hair follicle infundibulum and did not display a connection to the epidermis, as confirmed by examining serial sections (Figure 2B and S2).

Previous studies have found that *P53* mutations are common in human BCC and that loss of *p53* can promote BCCs in the IFE of irradiated *Ptch1*-heterozygous mice (Ponten et al., 1997; Wang et al., 2011). We therefore assessed tumor formation in *K14;Ptch1* mice that additionally harbored homozygous floxed alleles of *p53*. In mice biopsied up to 12 weeks after tamoxifen treatment, however, we observed that loss of *p53* did not enhance IFE tumorigenesis (Figure 2C). In stark contrast, *Gli1;Ptch1*, *Hes1;Ptch1* and *Lrig1;Ptch1* mice with wild-type *p53* all developed large hair follicle-associated lesions that filled the dermis within 5–7 weeks post-induction (Figure 1). These findings indicate that BCC-like tumors preferentially develop from hair follicle stem cells, and that loss of *p53* does not promote IFE tumor formation.

Hair follicle-derived tumors express similar markers irrespective of stem cell origin

Given our finding that BCC-like lesions can originate from multiple hair follicle stem cell populations, we next determined whether these tumors display differences in marker expression. Irregardless of cellular origin, all hair follicle-derived tumors consistently expressed K14 as well as K17, a Hh pathway target gene (Callahan et al., 2004) (Figure 3A–B). K17 was also upregulated throughout the hyperplastic epidermis of induced *K14;Ptch1* animals, indicating that IFE stem cells which had deleted *Ptch1* remained in the epidermis and activated downstream Hh signaling in spite of the absence of tumors.

All hair follicle-derived tumors also expressed the stem markers Sox9 and Lrig1 (Figure 3C–D). At the same time, these tumors sometimes exhibited signs of early differentiation, as evidenced by expression of K10 (Figure 3E). In contrast, Involucrin, a later differentiation marker, was not observed (Figure 3F). As we were ultimately unable to detect differential marker expression, this suggests that all hair follicle-derived tumors display a similar phenotype irrespective of cellular origin.

BCC-like tumors efficiently arise from stem cells within touch dome epithelia

Although the IFE was largely devoid of tumors, we noticed that *Gli1;Ptch1* mice frequently developed branched lesions that radiated down from the epidermis specifically at sites adjacent to guard hairs (Figure 4A). Since mechanosensory touch dome (TD) epithelia are localized to guard hairs, we reevaluated the activity of Gli1-Cre^{ERT2} by generating mice expressing the recombinase along with either an inducible *ROSA26R* promoter-driven β-galactosidase (LacZ) or YFP reporter allele (*Gli1;LacZ* or *Gli1;YFP*, respectively). After tamoxifen induction, these mice indeed displayed reporter gene expression in TDs, as

determined both by whole-mount staining for LacZ as well as by co-localizing YFP with K17, a marker of TDs (Doucet et al., 2013; Moll et al., 1993)(Figure 4B). TD labeling was stably maintained long-term (Figure 4B and S3), suggesting that TDs are renewed by dedicated stem cell pools that display Hh pathway activity during homeostasis.

It is interesting to note that normal TDs typically consist of keratinocytes displaying a columnar basal morphology resembling the peripheral palisades observed in hair follicle-associated BCC-like tumors (Figure 4C). To establish that epidermis-associated *Gli1;Ptch1* tumors are derived from TDs, we examined tumor formation at earlier timepoints and observed a gradual lateral as well as downward expansion of K17+ TD-derived cell clusters upon deletion of *Ptch1* (Figure 4D–E). Just as normal TDs are juxtaposed by innervated neuroendocrine Merkel cells (Moll et al., 2005), epidermis-associated tumors in *Gli1;Ptch1* mice were also lined by Merkel cells, as assessed by staining for the marker K8 (Figure 4D). In addition, neurofilament staining confirmed that tumor-associated Merkel cells were innervated by sensory afferents (Figure 4F). In contrast, Merkel cells were never detected near any hair follicle-associated tumors (data not shown).

Infrequently, we also observed more extensive epidermis-associated lesions in *K14;Ptch1* mice (Figure 4G). These tumors resembled those arising from the TD in *Gli1;Ptch1* animals, and staining for K8 confirmed the presence of Merkel cells localized to these tumors (Figure 4G). To assess whether K14-Cre^{ERT} can induce recombination in the TD, we analyzed mice expressing the recombinase along with the YFP reporter allele (*K14;YFP*). Indeed, TD epithelia were occasionally labeled in *K14;YFP* animals, although at a frequency that was significantly reduced compared to either IFE labeling outside of TDs, or labeling within TDs in *Gli1;YFP* mice (Figure 4H–I). Diminished K14-Cre^{ERT} activity in the TD is likely due to reduced expression of K14 in TDs relative to the rest of the IFE, which is apparent only upon high dilution (1:1,000,000) of an antibody against this keratin (Figure 4J). Altogether, our findings suggest that TD epithelia activate Hh signaling during homeostasis and, unlike the rest of the IFE, are highly susceptible to forming BCC-like lesions upon loss of *Ptch1*.

Surgical denervation inhibits tumorigenesis

Surgical nerve ablation has been reported to cause loss of TDs and Merkel cells in rodent and feline skin (English et al., 1983; Nurse et al., 1984). To confirm these findings, we denervated thoracic-level cutaneous nerves to one side of the dorsal midline in 6 week old wild-type mice, while leaving the contralateral side intact as a sham control. After collecting samples 3 or 5 weeks after surgery, we observed that denervated skin displayed a significant reduction in K17+ TD size and abundance (Figure 5A–B). Merkel cells were lost from denervated skin (Figure 5B), possibly subsequent to K17 downregulation (Figure S3), while remaining Merkel cells were frequently not innervated (Figure 5C). To further assess Hh activity after denervation, we denervated 6 week old *Gli1;LacZ* mice and treated these animals with tamoxifen 2 weeks after surgery (Figure 5D). Four days later, we harvested biopsies for LacZ staining and observed reduced TD labeling compared to intact contralateral control (Figure 5D). As K17 and Gli1 are both downstream targets of Hh signaling, these findings suggest that cutaneous nerves are crucial for maintaining Hh pathway activity in the TD niche.

We next extended these studies to determine whether denervation can inhibit TD-derived tumors in *Gli1;Ptch1* mice. To first confirm that denervation performed subsequent to tamoxifen induction does not affect Gli1-Cre^{ERT2} recombinase activity in the TD, we induced *Gli1;LacZ* mice with tamoxifen at 5.5 weeks of age, then subsequently denervated one side of the dorsal skin 4 days after induction (Figure 6A). Two weeks after nerve ablation, we harvested skin biopsies and observed similar patterns of LacZ staining in denervated and sham-operated skin (Figure 6A). Thus, while TD epithelia rely on nerves to activate Hh (Figures 5B, D), nerve ablation and consequent loss of Hh pathway activity do not immediately affect the abundance or distribution of already-labeled cells in the TD, which can persist for weeks without neural input (English et al., 1983; Nurse et al., 1984).

In *Gli1;Ptch1* mice, we utilized the same approach, inducing animals with tamoxifen at 5.5 weeks of age and subsequently denervating one side of the skin (Figure 6B). Two or five weeks after tamoxifen induction, we harvested biopsies and confirmed that cutaneous nerves were stably ablated (Figure S4). Although denervation did not affect tumor growth 2 weeks post-induction, we observed a significant inhibition of TD-derived tumors in denervated skin 5 weeks after tamoxifen treatment (Figure 6B–C). In 9 out of 10 mice, fewer TD-derived tumor cells were observed within denervated skin, compared to the contralateral sham control (mean = 81.3 vs. 35.3 TD-derived tumor cells/cm for sham vs. denervated skin, respectively; $p = 0.017$ by paired Student's *t*-test). In addition, the number of Merkel cells associated with these tumors was also reduced (Figure 6C). This effect was specific to TD-derived tumors, since nerve ablation did not significantly affect adjacent hair follicle-associated lesions (Figure 6D), arguing that denervation does not induce a systemic anti-tumorigenic response.

If epidermis-associated tumors which develop infrequently in *K14;Ptch1* mice are derived exclusively from TDs, denervation should also prevent BCC-like lesions in these animals. We therefore surgically removed the nerves from dorsal back skin in 6 week old *K14;Ptch1* mice, exposed these animals to tamoxifen 2 weeks after surgery, and harvested biopsies after an additional 5 weeks. Although nerve ablation did not affect K14-Cre^{ERT}-mediated recombination in the IFE (Figure 6E), the formation of rare TD-derived lesions was attenuated in denervated skin (mean = 20.7 vs. 3.9 TD-derived tumor cells/cm for sham vs. denervated skin, respectively; $p = 0.04$ by paired Student's *t*-test) (Figure 6F). In contrast, the formation of small ectopic buds along the IFE was unaffected. Together, our findings in *K14;Ptch1* and *Gli1;Ptch1* mice indicate that epidermis-associated tumors preferentially arise from TD epithelia, and that sensory nerves promote progression of TD-derived tumors.

The mechanosensory niche promotes tumorigenesis

How does the perineural microenvironment foster a pro-tumorigenic niche? As TDs display heightened *Gli1* expression, we investigated the possibility that paracrine signals released by nerves can promote canonical Hh signaling in the TD. In mammals, three Hh ligands—Shh, Dhh and Ihh—activate the pathway. After dissecting dorsal root ganglia, where cell bodies of cutaneous sensory nerves are located, we determined by qRT-PCR that these nerves express markedly higher levels of all three Hh ligands compared to skin epithelia (Figure 7A). These findings are concordant with recent data showing that neuron-specific loss of

Shh causes deterioration of TDs and Merkel cells in adult mice (Drs. Y. Xiao and I. Brownell, personal communication).

Although the loss of *Ptch1* may seemingly bypass the requirement for Hh ligands to induce pathway activity in TD-derived tumors, recent studies have shown that *Ptch1*-deficient skin upregulates a related protein, Ptch2, which can also bind Hh ligands and suppress downstream signaling (Adolphe et al., 2014). Indeed, we confirmed by qRT-PCR that *Ptch2* expression was increased upon deletion of *Ptch1* in *K14;Ptch1* mice, suggesting that Ptch2 may dampen Hh signaling in tumor-resistant IFE (Figure 7B).

To further elucidate why different skin compartments vary in tumor predisposition, we searched for molecular differences that might distinguish tumor-susceptible hair follicle and TD compartments, from tumor-resistant IFE. The cell surface glycoprotein CD200 is a marker of hair follicle stem cells in humans and may promote immune privilege in various organs (Garza et al., 2011). CD200 has also recently been found to be enriched in cells that can initiate BCC (Colmont et al., 2013). In mice, CD200 is a marker of TD epithelia (Woo et al., 2010), and we also observed CD200 throughout the hair follicle, but not in the IFE (Figure 7C). Furthermore, all hair follicle- and TD-derived tumors strongly expressed CD200, whereas strikingly, CD200 was completely absent from hyperplastic IFE or weakly expressed in ectopic IFE buds in *K14;Ptch1* mice (Figure 7D). In keratinocytes, either loss of *Ptch1* or pharmacological activation of Hh signaling elevated *CD200* (Figure 7E–F). Together, these findings suggest that in tumor-resistant IFE, loss of *Ptch1* only partially activates the Hh signaling program, leading to upregulation of some target genes (*Gli1*, *Ptch2*, K17), but not others (CD200) (Figure 7B and S5). Within the TD niche, nerve-derived factors, possibly involving Hh ligands, may potentiate full pathway activation and tumorigenesis. Notably, as normal TDs resemble BCCs in terms of basal columnar morphology as well as elevated baseline expression of *Gli1*, K17 and CD200, this once again argues that TDs are “hot spots” in the epidermis that are primed for tumor formation.

DISCUSSION

The precise cellular origin of BCC has been controversial, as recent studies have seemingly yielded diametrically opposed results. Whereas SmoM2-induced BCC-like tumors appear to arise from stem cells in the IFE, but not from the hair follicle bulge (Wong and Reiter, 2011; Youssef et al., 2010), tumors driven by loss of *Ptch1* have been reported to originate from the bulge and secondary hair germ, but not the IFE (Kasper et al., 2011; Wang et al., 2011). Our results are concordant with those of Wang et al., and Kasper et al., although we have identified additional stem cell populations that are also susceptible to tumorigenesis. Altogether, using a mouse model that recapitulates the most common genetic aberration seen in human BCCs, our findings indicate that these tumors preferentially arise from stem cells located specifically in the upper bulge, lower bulge/secondary hair germ, isthmus and TD, but not from IFE stem cells or transit-amplifying matrix cells (Figure 7G).

What predisposes certain cutaneous epithelia to forming tumors upon loss of *Ptch1*? Previous studies have postulated that degradation of Gli proteins may restrict Hh signaling and BCC formation in the skin (Huntzicker et al., 2006; Oro and Higgins, 2003). Supportive

of this, Grachtchouk et al., has shown that upon forced activation of downstream Hh signaling, BCC-like tumors can arise from both hair follicles and IFE (Grachtchouk et al., 2011). Alternatively, upregulation of Ptch2 in the absence of Ptch1 may also restrain full Hh pathway activity. Indeed, Adolphe et al., has recently demonstrated that mice lacking both Ptch1 and Ptch2 develop a more severe hyperplastic and BCC-like invaginating epidermal phenotype than do mice deficient for Ptch1 alone (Adolphe et al., 2014). Our findings are concordant with these observations and suggest that tumor-resistant IFE cells become oncogenic only upon high activation of Hh signaling requiring loss of multiple redundant inhibitors of the pathway. These data further suggest that sites in the skin which normally display high level Hh signaling are likely predisposed to BCC formation, and that loss of *Ptch1* alone at these sites is sufficient for tumorigenesis.

Consistent with this concept, we have found that TD epithelia display activated Hh signaling during homeostasis and are highly susceptible to forming tumors. Under normal conditions, TDs function as mechanosensory organs that detect light touch and transduce signals via underlying Merkel cells to slowly adapting type 1 sensory afferents (Maksimovic et al., 2014; Maricich et al., 2009). We have further shown that cutaneous sensory nerves express Hh ligands, and that denervation impairs Hh activity in the TD and inhibits the progression of TD-derived tumors. While these results suggest that nerve endings secrete Hh ligands to promote TD-derived tumors, it is important to add, however, that TD-derived tumors did not appear to respond to a neutralizing antibody generated against Shh (Figure S6). These results might be explained if multiple Hh ligands simultaneously promote TD-derived tumors, and tumor inhibition can be achieved only by complete and sustained impairment of Hh signaling, as might occur following long-term denervation. These findings do not rule out the possibility that nerves may also non-canonically activate downstream Hh signaling via pathways such as TGF-β (Nolan-Stevaux et al., 2009). Alternatively, cutaneous nerves are known to secrete cytokines such as Calcitonin gene-related peptide as well as Substance P, which can serve functional roles during epidermal development and pathology (Lumpkin et al., 2010). Indeed, neural changes are often observed in patients with psoriasis and atopic eczema, and nerve removal inhibits the epidermal hyperplasia observed in experimental models of these diseases (Ostrowski et al., 2011; Ward et al., 2012).

Our findings complement previous studies showing that nerves can influence tumors in other organs. For instance, chemical denervation can inhibit tumorigenesis in the stomach and colon (Polli-Lopes et al., 2003). More recent studies in prostate cancer have found that peritumoral sympathetic nerves promote tumor growth, while intratumoral parasympathetic nerves stimulate metastasis (Magnon et al., 2013). In addition, β-blockers, which interfere with the sympathetic nervous system, can delay progression of various cancers (Lemeshow et al., 2011). A tumor-modulatory role for nerves has not been described for Merkel cell carcinoma, a rare cancer thought to originate from Merkel cells, but would not be surprising given the close association between nerve endings and mechanosensory cells.

In human, BCCs primarily develop in sun-exposed, hair-bearing skin. In addition, the majority of tumors (between 57–78%) typically display a nodular phenotype, while only a minority (15–16%) present as superficial lesions (Bastiaens et al., 1998; Scrivener et al., 2002). Interestingly, Grachtchouk et al., has previously noted in mice that tumors originating

from hair follicles appear nodular, whereas IFE-associated tumors resemble superficial human BCCs, suggesting that tumor histologic phenotype can reflect cellular origin (Grachtchouk et al., 2011). From this perspective, the high prevalence of nodular human BCCs is consistent with our finding that hair follicle stem cells likely serve as the primary progenitors for these tumors. While our studies do not exclude the possibility that loss of *Ptch1* may give rise to tumors from the IFE after an extended latency, our findings also suggest that some human BCCs that appear to arise from the IFE might actually originate from the TD.

Since Merkel cells are invariably associated with TD-derived tumors in our studies, we also examined the distribution of these cells in a limited number of human BCC samples. In 4/10 tumors, we observed clusters of Merkel cells located within small tumor foci from both superficial and deeper lesions, but not within larger tumor masses (Figure 7H and S7). These observations are consistent with a potential mechanosensory niche for BCC, or possibly even “micro-niches” within the immediately vicinity of innervated Merkel cells, which in humans are widely distributed not just in TDs, but also throughout the skin and hair follicles (Lacour et al., 1991). Moreover, these cells are particularly abundant in glabrous skin (Fradette et al., 1995), where palmoplantar pits frequently develop in Gorlin’s patients. Merkel cells have also been observed in a minority of human BCCs, including a subtype known as fibroepithelioma of Pinkus (Sellheyer and Nelson, 2011; Sellheyer et al., 2011), but are more commonly associated with trichoblastoma (Schulz and Hartschuh, 1997). It remains to be seen whether Merkel cells play an early supporting role during BCC tumor initiation, but are subsequently lost as the tumor expands. Further work will be required to determine whether both Merkel cells and nerves preferentially associate with specific BCC subtypes, or possibly early during tumorigenesis, and if so, whether targeting these niche elements might represent a viable therapeutic strategy.

EXPERIMENTAL PROCEDURES

Animals

The following mice were used: *Gli1*$^{tm3(cre/ERT2)Alj}$ (Ahn and Joyner, 2004); *Tg(KRT14-cre/ERT)20Efu* (Vasioukhin et al., 1999); *Hes1*$^{tm1(cre/ERT2)Lcm}$ (Kopinke et al., 2011); *Lrig1*$^{tm1.1(cre/ERT2)Rjc}$ (Powell et al., 2012); *FVB.Cg-Tg(KRT1-5-cre)5132Jlj/Mmnc* (Berton et al., 2003); *Gt(ROSA)26Sor*^{tm1Sor} (Soriano, 1999); *Gt(ROSA)26Sor*$^{tm1(EYFP)Cos}$ (Srinivas et al., 2001); *Ptch1*^{tm1Hahn} (Uhmann et al., 2007); and *Trp53*^{tm1Brn} (Marino et al., 2000).

Mouse Manipulations

For tumor cell-of-origin experiments, animals were induced with tamoxifen at 7.5 weeks of age. For nerve studies, mice were induced and denervated according to the schedules described in the text. Tamoxifen doses are as follows: 1 dose at 5 mg per 40 grams body weight for *Gli1;Ptch1* and *Hes1;Ptch1* mice; one dose at 1 mg per 40 grams body weight for *Lrig1;Ptch1* mice; and three daily doses, each 1 mg per 40 grams body weight, for *K14;Ptch1* mice. Skin biopsies were harvested as described (Wong and Reiter, 2011). Denervation was adapted from previously described procedures (Ostrowski et al., 2011). Briefly, mice were anesthetized, and a 4.5–5 cm incision was made along the dorsal midline

to expose cutaneous nerves on the left side (T3-12). These were blunt dissected close to their anatomical entry into the skin, while nerves on the right side were left intact. All studies were performed in accordance with regulations established by the University of Michigan Unit for Laboratory Animal Medicine.

Tissue Staining

Biopsies were fixed for 1 hour in cold 3.7% paraformaldehyde, incubated overnight in 30% sucrose at 4 degrees, before embedding in OCT. Frozen sections were stained using standard protocols with the following antibodies: anti-K17 (D73C7, 1:1,500, Cell Signaling); anti-K8 (TROMA-I, 1:500, Developmental Studies Hybridoma Bank); anti-K20 (D409, 1:500, American Research Products); anti-K14 (AF64, 1:1,000,000, Covance); anti-K5 (03-GP-CK5, American Research Products); anti-GFP/YFP (GFP-1020, 1:2,000, Aves Labs); anti-NF (C28E10, 1:500, Cell Signaling); anti-β4 (346-11A, 1:500, BD Pharmingen); anti-Sox9 (H-90, 1:150, Santa Cruz Biotechnology); anti-Lrig1 (AF3688, 1:25, R&D Systems); anti-K10 (PRB-159P, 1:500, Covance); anti-Involucrin (PRB-140C, 1:500, Covance); anti-Chromogranin A (24-1113C1, 1:250, American Research Products); and anti-CD200 eFluor660 (OX90, 1:2,000, eBioscience). For frozen samples stained for YFP, sections were pre-treated with cold methanol for 5 minutes prior to blocking. For whole-mount β-gal staining, *in situ* staining and qPCR, see Supplemental Information. Image processing was performed using Adobe Photoshop CS6, with the Auto-Blend function applied to maximize image sharpness across focal planes in the same microscopic field.

Quantitation

For TDs and TD-derived tumors, 15 non-consecutive frozen sections (each 10 um thick, ~1 cm in length) were analyzed. TDs were identified based on columnar morphology, K17 expression and association with K8-expressing Merkel cells. TD size was assessed by counting the number of K17+ cells within each cluster along ~15 cm of skin. TD-derived tumors were identified based on criteria used for normal TDs, and the total number of K17+ cells within lesions radiating down from the epidermis was scored. K17-expressing cells in the infundibulum were excluded (Veniaminova et al., 2013). K17 expression is absent in normal non-TD IFE. To quantitate hair follicle-associated tumors in *Gli1;Ptch1* mice, we measured tumor volumes from 5 non-consecutive frozen sections (10 um thick, ~1 cm in length) for each sample. We performed IHC for K17, outlined tumors in Photoshop, and recorded tumor area in pixels. For quantitating ectopic hair buds in *K14;Ptch1* mice, we counted the number of cell clusters, defined as consisting of at least 3 continuous K17+ cells, along the entire IFE.

Human Samples

Human BCCs were obtained with informed consent under IRB #HUM00042233, in accordance with procedures approved by the Institutional Review Board of the University of Michigan Medical School. Tumor biopsies were processed for paraffin sections and de-identified, and thus not regulated as per IRB guidelines (exempt IRB protocol HUM00051875).

Statistics

A paired Student's *t*-Test was used to assess significance in experiments where denervated and sham-operated, matched skin samples were harvested from the same animal. For all other experiments, an unpaired Student's *t*-Test was used. Calculations were performed at http://www.physics.csbsju.edu/stats/Index.html.

Supplementary Material

Refer to Web version on PubMed Central for supplementary material.

Acknowledgments

We are grateful to Dr. Isaac Brownell (NCI) for helpful discussions; to the Dlugosz lab at the University of Michigan for sharing reagents; and to Nisha Meireles, University of Michigan Skin Cancer Biobank, for Biobank coordination and management. S.Y.W. acknowledges the support of the National Institutes of Health/NIAMS (R00AR059796, R01AR065409); the University of Michigan Department of Dermatology; the Biological Sciences Scholars Program; the Center for Organogenesis; the UM Comprehensive Cancer Center; and the John S. and Suzanne C. Munn Cancer Fund. This work was also supported in part by NIAMS R01AR063437, R01AR062546 and R21AR063852 to N.L.W.; by NIAMS R01AR045973 and NCI R01CA087837 to A.A.D.; and by NIGMS T32 GM007315 to S.C.P.

References

Adolphe C, Nieuwenhuis E, Villani R, Li ZJ, Kaur P, Hui CC, Wainwright B. Patched1 and Patched2 redundancy plays a key role in regulating epidermal differentiation. J Invest Dermatol. 2014; 134:1981–1990. [PubMed: 24492243]

Ahn S, Joyner AL. Dynamic changes in the response of cells to positive hedgehog signaling during mouse limb patterning. Cell. 2004; 118:505–516. [PubMed: 15315762]

Aszterbaum M, Epstein J, Oro A, Douglas V, LeBoit PE, Scott MP, Epstein EH Jr. Ultraviolet and ionizing radiation enhance the growth of BCCs and trichoblastomas in patched heterozygous knockout mice. Nat Med. 1999; 5:1285–1291. [PubMed: 10545995]

Bastiaens MT, Hoefnagel JJ, Bruijn JA, Westendorp RG, Vermeer BJ, Bouwes Bavinck JN. Differences in age, site distribution, and sex between nodular and superficial basal cell carcinoma indicate different types of tumors. J Invest Dermatol. 1998; 110:880–884. [PubMed: 9620293]

Berton TR, Matsumoto T, Page A, Conti CJ, Deng CX, Jorcano JL, Johnson DG. Tumor formation in mice with conditional inactivation of Brca1 in epithelial tissues. Oncogene. 2003; 22:5415–5426. [PubMed: 12934101]

Bonifas JM, Bare JW, Kerschmann RL, Master SP, Epstein EH Jr. Parental origin of chromosome 9q22.3-q31 lost in basal cell carcinomas from basal cell nevus syndrome patients. Hum Mol Genet. 1994; 3:447–448. [PubMed: 8012356]

Brownell I, Guevara E, Bai CB, Loomis CA, Joyner AL. Nerve-derived sonic hedgehog defines a niche for hair follicle stem cells capable of becoming epidermal stem cells. Cell Stem Cell. 2011; 8:552–565. [PubMed: 21549329]

Callahan CA, Ofstad T, Horng L, Wang JK, Zhen HH, Coulombe PA, Oro AE. MIM/BEG4, a Sonic hedgehog-responsive gene that potentiates Gli-dependent transcription. Genes Dev. 2004; 18:2724–2729. [PubMed: 15545630]

Colmont CS, Benketah A, Reed SH, Hawk NV, Telford WG, Ohyama M, Udey MC, Yee CL, Vogel JC, Patel GK. CD200-expressing human basal cell carcinoma cells initiate tumor growth. Proc Natl Acad Sci USA. 2013; 110:1434–1439. [PubMed: 23292936]

Doucet YS, Woo SH, Ruiz ME, Owens DM. The touch dome defines an epidermal niche specialized for mechanosensory signaling. Cell Rep. 2013; 3:1759–1763. [PubMed: 23727240]

English KB, Kavka-Van Norman D, Horch K. Effects of chronic denervation in type I cutaneous mechanoreceptors (Haarscheiben). Anat Rec. 1983; 207:79–88. [PubMed: 6638534]

Epstein EH. Basal cell carcinomas: attack of the hedgehog. Nat Rev Cancer. 2008; 8:743–754. [PubMed: 18813320]

Epstein EH Jr. Mommy - where do tumors come from? J Clin Invest. 2011; 121:1681–1683. [PubMed: 21519146]

Fradette J, Godbout MJ, Michel M, Germain L. Localization of Merkel cells at hairless and hairy human skin sites using keratin 18. Biochem Cell Biol. 1995; 73:635–639. [PubMed: 8714683]

Garza LA, Yang CC, Zhao T, Blatt HB, Lee M, He H, Stanton DC, Carrasco L, Spiegel JH, Tobias JW, et al. Bald scalp in men with androgenetic alopecia retains hair follicle stem cells but lacks CD200-rich and CD34-positive hair follicle progenitor cells. J Clin Invest. 2011; 121:613–622. [PubMed: 21206086]

Grachtchouk M, Mo R, Yu S, Zhang X, Sasaki H, Hui CC, Dlugosz AA. Basal cell carcinomas in mice overexpressing Gli2 in skin. Nat Genet. 2000; 24:216–217. [PubMed: 10700170]

Grachtchouk M, Pero J, Yang SH, Ermilov AN, Michael LE, Wang A, Wilbert D, Patel RM, Ferris J, Diener J, et al. Basal cell carcinomas in mice arise from hair follicle stem cells and multiple epithelial progenitor populations. J Clin Invest. 2011; 121:1768–1781. [PubMed: 21519145]

Hahn H, Wicking C, Zaphiropoulous PG, Gailani MR, Shanley S, Chidambaram A, Vorechovsky I, Holmberg E, Unden AB, Gillies S, et al. Mutations of the human homolog of Drosophila patched in the nevoid basal cell carcinoma syndrome. Cell. 1996; 85:841–851. [PubMed: 8681379]

Huntzicker EG, Estay IS, Zhen H, Lokteva LA, Jackson PK, Oro AE. Dual degradation signals control Gli protein stability and tumor formation. Genes Dev. 2006; 20:276–281. [PubMed: 16421275]

Jaks V, Kasper M, Toftgård R. The hair follicle - a stem cell zoo. Exp Cell Res. 2010; 316:1422–1428. [PubMed: 20338163]

Jih DM, Lyle S, Elenitsas R, Elder DE, Cotsarelis G. Cytokeratin 15 expression in trichoepitheliomas and a subset of basal cell carcinomas suggests they originate from hair follicle stem cells. J Cutan Pathol. 1999; 26:113–118. [PubMed: 10235375]

Johnson RL, Rothman AL, Xie J, Goodrich LV, Bare JW, Bonifas JM, Quinn AG, Myers RM, Cox DR, Epstein EH Jr, et al. Human homolog of patched, a candidate gene for the basal cell nevus syndrome. Science. 1996; 272:1668–1671. [PubMed: 8658145]

Kasper M, Jaks V, Are A, Bergström Å, Schwäger A, Barker N, Toftgård R. Wounding enhances epidermal tumorigenesis by recruiting hair follicle keratinocytes. Proc Natl Acad Sci USA. 2011; 108:4099–4104. [PubMed: 21321199]

Kasper M, Jaks V, Hohl D, Toftgård R. Basal cell carcinoma - molecular biology and potential new therapies. J Clin Invest. 2012; 122:455–463. [PubMed: 22293184]

Kopinke D, Brailsford M, Shea JE, Leavitt R, Scaife CL, Murtaugh LC. Lineage tracing reveals the dynamic contribution of Hes1+ cells to the developing and adult pancreas. Development. 2011; 138:431–441. [PubMed: 21205788]

Lacour JP, Dubois D, Pisani A, Ortonne JP. Anatomical mapping of Merkel cells in normal human adult epidermis. Br J Dermatol. 1991; 125:535–542. [PubMed: 1722110]

Lemeshow S, Sørensen HT, Phillips G, Yang EV, Antonsen S, Riis AH, Lesinski GB, Jackson R, Glaser R. β-Blockers and survival among Danish patients with malignant melanoma: a population-based cohort study. Cancer Epidemiol Biomarkers Prev. 2011; 20:2273–2279. [PubMed: 21933972]

Lumpkin EA, Marshall KL, Nelson AM. The cell biology of touch. J Cell Biol. 2010; 191:237–248. [PubMed: 20956378]

Magnon C, Hall SJ, Lin J, Xue X, Gerber L, Freedland SJ, Frenette PS. Autonomic nerve development contributes to prostate cancer progression. Science. 2013; 341:1236361. [PubMed: 23846904]

Maksimovic S, Nakatani M, Baba Y, Nelson AM, Marshall KL, Wellnitz SA, Firozi P, Woo SH, Ranade S, Patapoutian A, et al. Epidermal Merkel cells are mechanosensory cells that tune mammalian touch receptors. Nature. 2014; 509:617–621. [PubMed: 24717432]

Mao J, Ligon KL, Rakhlin EY, Thayer SP, Bronson RT, Rowitch D, McMahon AP. A novel somatic mouse model to survey tumorigenic potential applied to the Hedgehog pathway. Cancer Res. 2006; 66:10171–10178. [PubMed: 17047082]

Maricich SM, Wellnitz SA, Nelson AM, Lesniak DR, Gerling GJ, Lumpkin EA, Zoghbi HY. Merkel cells are essential for light-touch responses. Science. 2009; 324:1580–1582. [PubMed: 19541997]

Marino S, Vooijs M, van Der Gulden H, Jonkers J, Berns A. Induction of medulloblastomas in p53-null mutant mice by somatic inactivation of Rb in the external granular layer cells of the cerebellum. Genes Dev. 2000; 14:994–1004. [PubMed: 10783170]

Moll I, Roessler M, Brandner JM, Eispert AC, Houdek P, Moll R. Human Merkel cells - aspects of cell biology, distribution and functions. Eur J Cell Biol. 2005; 84:259–271. [PubMed: 15819406]

Moll I, Troyanovsky SM, Moll R. Special program of differentiation expressed in keratinocytes of human haarscheiben: an analysis of individual cytokeratin polypeptides. J Invest Dermatol. 1993; 100:69–76. [PubMed: 7678634]

Nilsson M, Unden AB, Krause D, Malmqwist U, Raza K, Zaphiropoulos PG, Toftgård R. Induction of basal cell carcinomas and trichoepitheliomas in mice overexpressing Gli-1. Proc Natl Acad Sci USA. 2000; 97:3438–3443. [PubMed: 10725363]

Nitzki F, Becker M, Frommhold A, Schulz-Schaeffer W, Hahn H. Patched knockout mouse models of basal cell carcinoma. J Skin Cancer. 2012; 2012:907543. [PubMed: 23024864]

Nolan-Stevaux O, Lau J, Truitt ML, Chu GC, Hebrok M, Fernández-Zapico ME, Hanahan D. GLI1 is regulated through Smoothened-independent mechanisms in neoplastic pancreatic ducts and mediates PDAC cell survival and transformation. Genes Dev. 2009; 23:24–36. [PubMed: 19136624]

Nurse CA, Macintyre L, Diamond J. A quantitative study of the time course of the reduction in Merkel cell number within denervated rat touch domes. Neuroscience. 1984; 11:521–533. [PubMed: 6717802]

Oro AE, Higgins K. Hair cycle regulation of Hedgehog signal reception. Dev Biol. 2003; 255:238–248. [PubMed: 12648487]

Oro AE, Higgins KM, Hu Z, Bonifas JM, Epstein EH Jr, Scott MP. Basal cell carcinomas in mice overexpressing sonic hedgehog. Science. 1997; 276:817–821. [PubMed: 9115210]

Ostrowski SM, Belkadi A, Loyd CM, Diaconu D, Ward NL. Cutaneous denervation of psoriasiform mouse skin improves acanthosis and inflammation in a sensory neuropeptide-dependent manner. J Invest Dermatol. 2011; 131:1530–1538. [PubMed: 21471984]

Page ME, Lombard P, Ng F, Gottgens B, Jensen KB. The epidermis comprises autonomous compartments maintained by distinct stem cell populations. Cell Stem Cell. 2013; 13:1–12. [PubMed: 23827700]

Polli-Lopes AC, Zucoloto S, de Queirós Cunha F, da Silva Figueiredo LA, Garcia SB. Myenteric denervation reduces the incidence of gastric tumors in rats. Cancer Lett. 2003; 190:45–50. [PubMed: 12536076]

Ponten F, Berg C, Ahmadian A, Ren ZP, Nister M, Lundeberg J, Uhlen M, Ponten J. Molecular pathology in basal cell cancer with p53 as a genetic marker. Oncogene. 1997; 15:1059–1067. [PubMed: 9285560]

Powell AE, Wang Y, Li Y, Poulin EJ, Means AL, Washington MK, Higginbotham JN, Juchheim A, Prasad N, Levy SE, et al. The pan-ErbB negative regulator Lrig1 is an intestinal stem cell marker that functions as a tumor suppressor. Cell. 2012; 149:146–158. [PubMed: 22464327]

Schirren CG, Rütten A, Kaudewitz P, Diaz C, McClain S, Burgdorf WH. Trichoblastoma and basal cell carcinoma are neoplasms with follicular differentiation sharing the same profile of cytokeratin intermediate filaments. Am J Dermatopathol. 1997; 19:341–350. [PubMed: 9261468]

Schulz T, Hartschuh W. Merkel cells are absent in basal cell carcinomas but frequently found in trichoblastomas. An immunohistochemical study. J Cutan Pathol. 1997; 24:14–24. [PubMed: 9027628]

Scrivener Y, Grosshans E, Cribier B. Variations of basal cell carcinomas according to gender, age, location and histopathological subtype. Br J Dermatol. 2002; 147:41–47. [PubMed: 12100183]

Sellheyer K, Nelson P. Follicular stem cell marker PHLDA1 (TDAG51) is superior to cytokeratin-20 in differentiating between trichoepithelioma and basal cell carcinoma in small biopsy specimens. J Cutan Pathol. 2011; 38:542–550. [PubMed: 21352265]

Sellheyer K, Nelson P, Kutzner H. Fibroepithelioma of Pinkus is a true basal cell carcinoma developing in association with a newly identified tumour-specific type of epidermal hyperplasia. Br J Dermatol. 2011; 166:88–97. [PubMed: 21910710]

Soriano P. Generalized lacZ expression with the ROSA26 Cre reporter strain. Nat Genet. 1999; 21:70–71. [PubMed: 9916792]

Srinivas S, Watanabe T, Lin CS, William CM, Tanabe Y, Jessell TM, Costantini F. Cre reporter strains produced by targeted insertion of EYFP and ECFP into the ROSA26 locus. BMC Dev Biol. 2001; 1:4. [PubMed: 11299042]

Uhmann A, Dittmann K, Nitzki F, Dressel R, Koleva M, Frommhold A, Zibat A, Binder C, Adham I, Nitsche M, et al. The Hedgehog receptor Patched controls lymphoid lineage commitment. Blood. 2007; 110:1814–1823. [PubMed: 17536012]

Vasioukhin V, Degenstein L, Wise B, Fuchs E. The magical touch: genome targeting in epidermal stem cells induced by tamoxifen application to mouse skin. Proc Natl Acad Sci USA. 1999; 96:8551–8556. [PubMed: 10411913]

Veniaminova NA, Vagnozzi AN, Kopinke D, Do TT, Murtaugh LC, Maillard I, Dlugosz AA, Reiter JF, Wong SY. Keratin 79 identifies a novel population of migratory epithelial cells that initiates hair canal morphogenesis and regeneration. Development. 2013; 140:4870–4880. [PubMed: 24198274]

Wang GY, Wang J, Mancianti ML, Epstein EH Jr. Basal cell carcinomas arise from hair follicle stem cells in Ptch1+/− mice. Cancer Cell. 2011; 19:1–11. [PubMed: 21251607]

Ward NL, Kavlick KD, Diaconu D, Dawes SM, Michaels KA, Gilbert E. Botulinum neurotoxin A decreases infiltrating cutaneous lymphocytes and improves acanthosis in the KC-Tie2 mouse model. J Invest Dermatol. 2012; 132:1927–1930. [PubMed: 22418873]

Wong SY, Reiter JF. Wounding mobilizes hair follicular stem cells to form tumors. Proc Natl Acad Sci USA. 2011; 108:4093–4098. [PubMed: 21321207]

Woo SH, Stumpfova M, Jensen UB, Lumpkin EA, Owens DM. Identification of epidermal progenitors for the Merkel cell lineage. Development. 2010; 137:3965–3971. [PubMed: 21041368]

Xie J, Murone M, Luoh SM, Ryan A, Gu Q, Zhang C, Bonifas JM, Lam CW, Hynes M, Goddard A, et al. Activating Smoothened mutations in sporadic basal-cell carcinoma. Nature. 1998; 391:90–92. [PubMed: 9422511]

Youssef KK, Keymeulen AV, Lapouge G, Beck B, Michaux C, Achouri Y, Sotiropoulou PA, Blanpain C. Identification of the cell lineage at the origin of basal cell carcinoma. Nat Cell Biol. 2010; 12:299–305. [PubMed: 20154679]

Zhang YV, Cheong J, Ciapurin N, McDermitt DJ, Tumbar T. Distinct self-renewal and differentiation phases in the niche of infrequently dividing hair follicle stem cells. Cell Stem Cell. 2009; 5:1–12. [PubMed: 19570504]

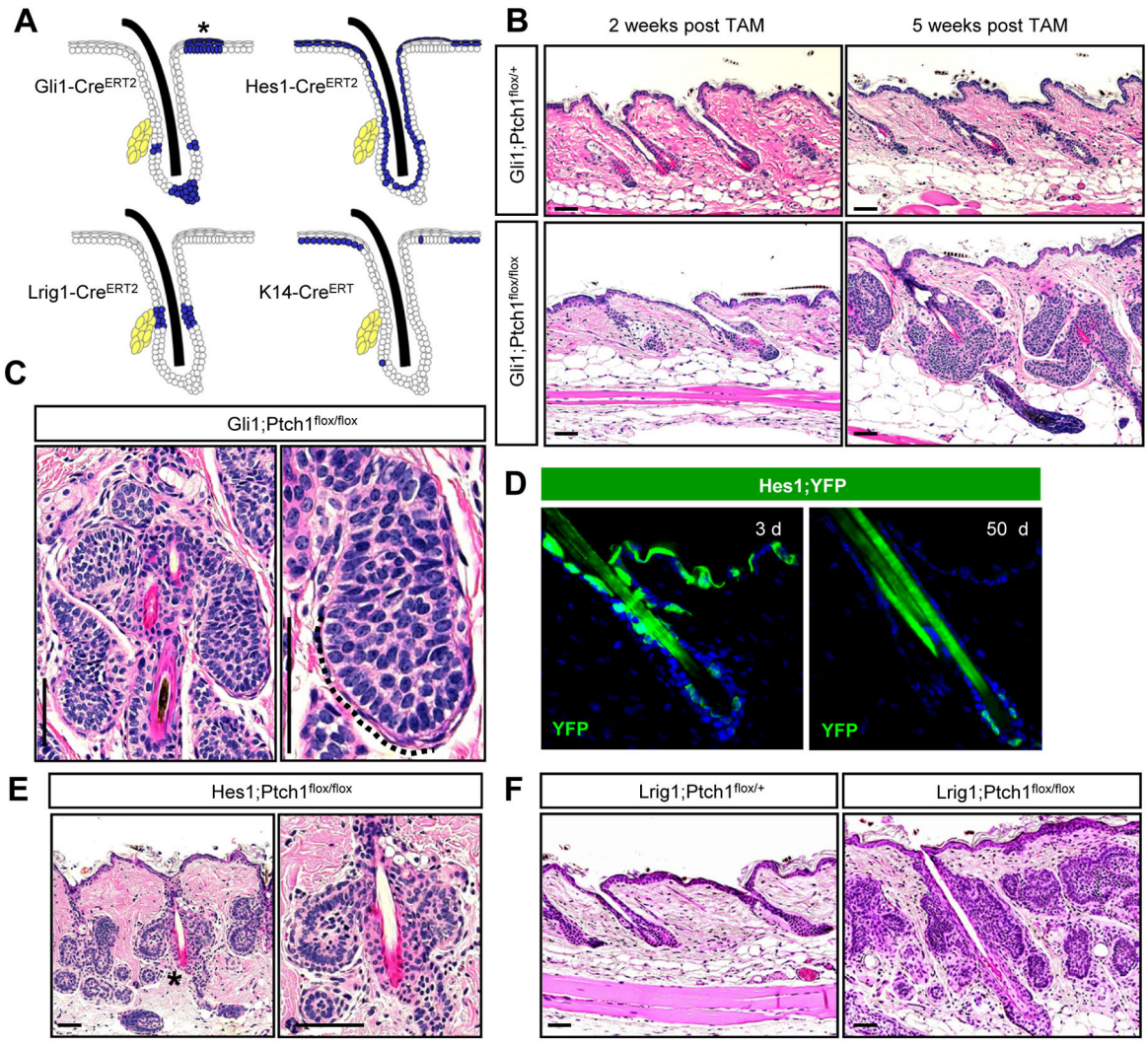

Figure 1. Multiple hair follicle stem cells readily form BCC-like tumors

A. Schematic showing areas of activity (blue) for the different inducible Cre recombinases used in this study. (*), TD epithelia. Yellow, sebaceous glands. **B.** Hematoxylin & eosin (H&E) staining showing that *Gli1;Ptch1* mice, but not control animals, develop numerous hair follicle-associated tumors, 5 weeks after tamoxifen (TAM). **C.** Higher magnification views of hair follicle-associated tumors with peripheral palisading (dotted line). **D.** Hes1-Cre^{ERT2}-mediated recombination of a floxed YFP reporter allele (green) in suprabasal cells of the epidermis, infundibulum and, less frequently, in the bulge, 3 days (left) or 50 days (right) post-TAM. **E.** *Hes1;Ptch1* mice develop bulge-associated tumors, 7 weeks post-TAM. Right panel is a higher magnification view of (*). **F.** *Lrig1;Ptch1* mice develop tumors associated with the isthmus and infundibulum, 5 weeks post-TAM. Scale bars, 50 μm. See also Figure S1.

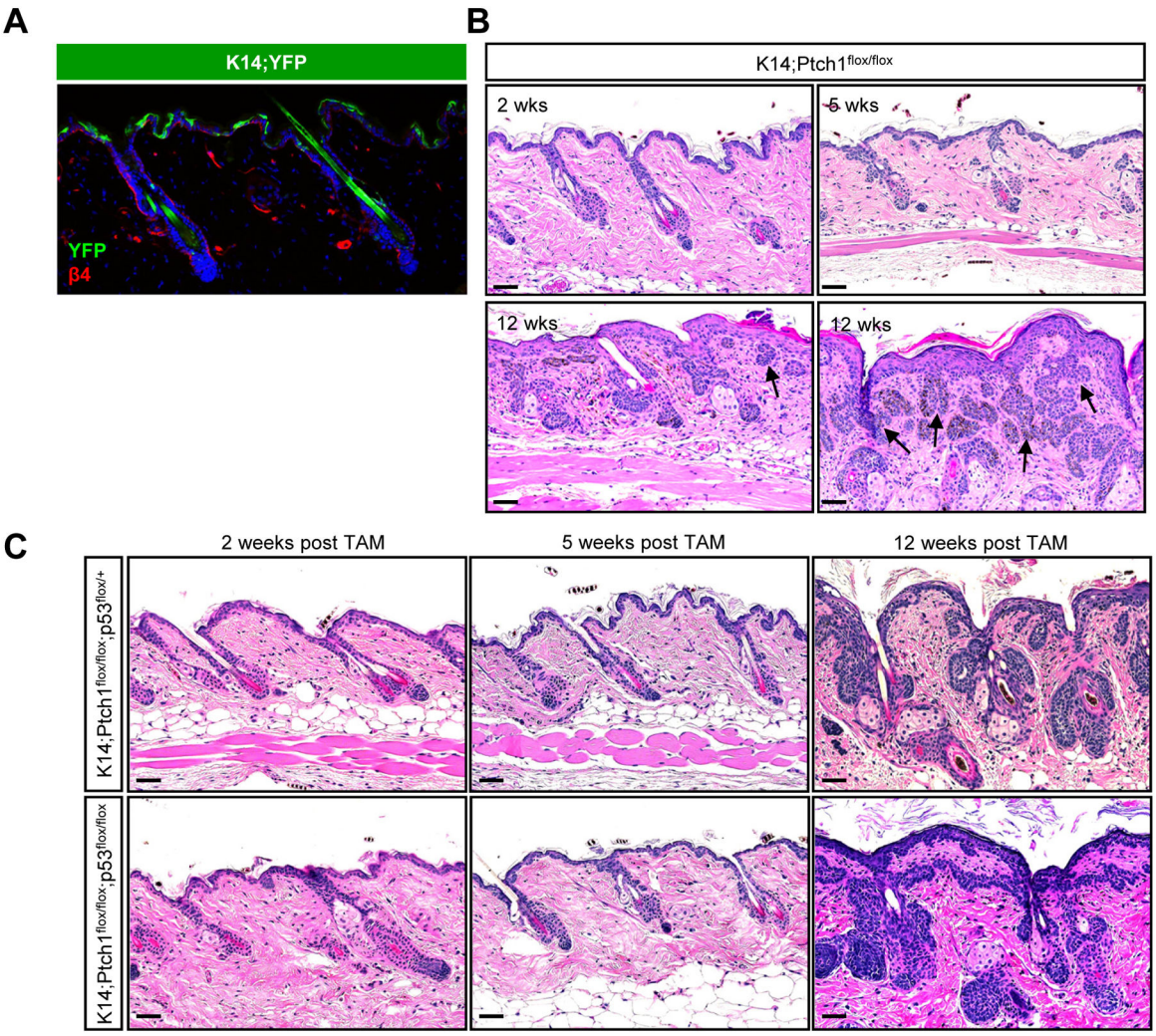

Figure 2. IFE stem cells do not efficiently form tumors

A. IHC showing that K14-Cre^{ERT} induces recombination of a YFP reporter allele (green) primarily in basal IFE cells, as marked by integrin β4 (red). **B.** *K14;Ptch1* mice develop small ectopic IFE-associated buds, 5 weeks after TAM. By 12 weeks post-TAM, the IFE is hyperplastic but largely devoid of lesions. Tumors adjacent to the IFE (arrows) are typically connected to hair follicles, as shown in serial sections (Figure S2). **C.** Loss of *p53* does not promote IFE tumor formation, 12 weeks post-TAM. Scale bars, 50 μm.

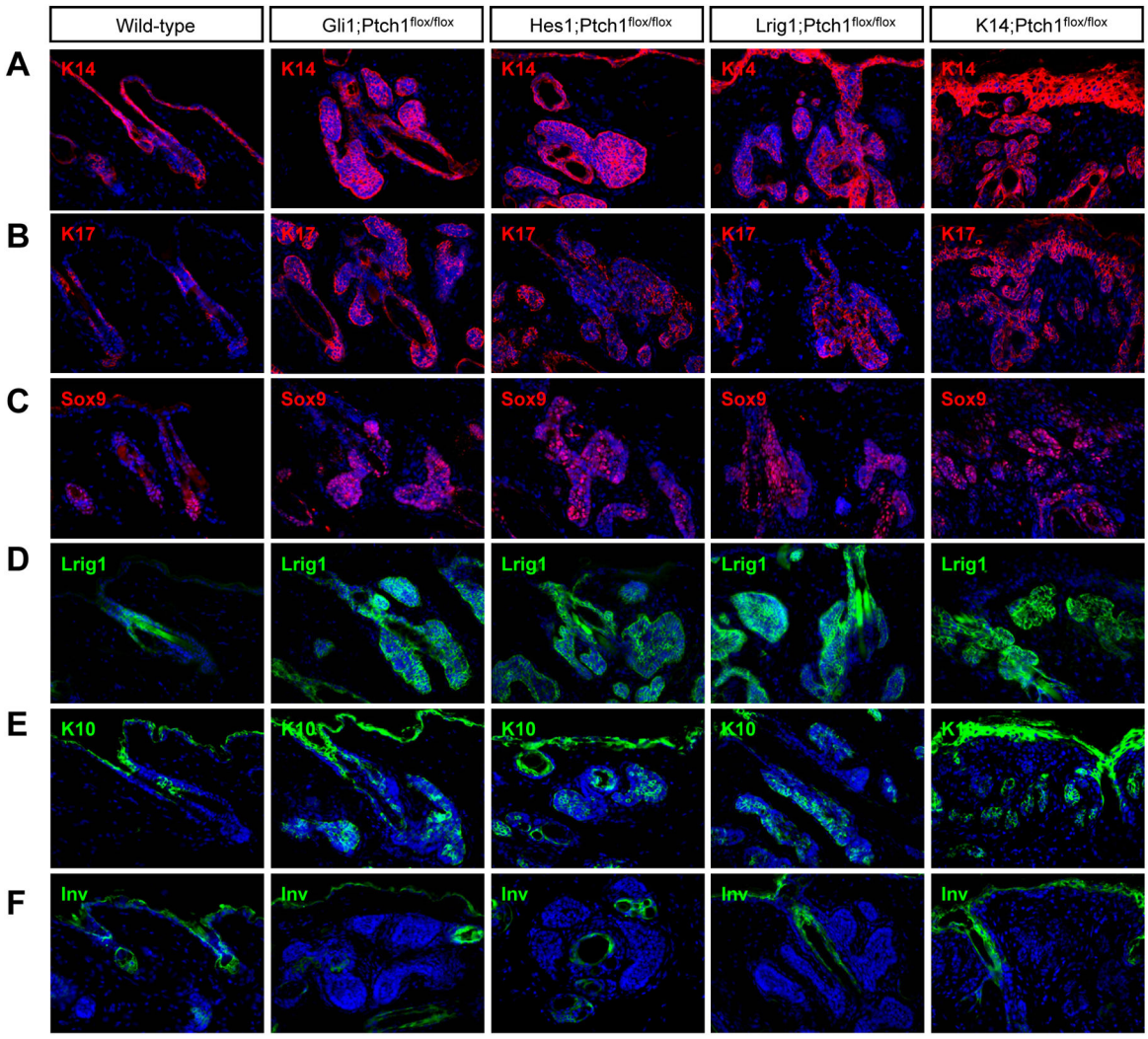

Figure 3. Hair follicle-derived tumors express similar markers regardless of cellular origin

IHC for **(A)** K14, **(B)** K17, **(C)** Sox9, **(D)** Lrig1, **(E)** K10, and **(F)** Involucrin (Inv). Wild-type telogen hair follicles were from 7.5 week old mice. *Gli1;Ptch1* and *Lrig1;Ptch1* tumors were collected 5 weeks post-TAM, while *Hes1;Ptch1* and *K14;Ptch1* samples were harvested 7 and 12 weeks post-TAM, respectively. Arrows indicate follicles where the bulge is visible. Scale bars, 50 μm.

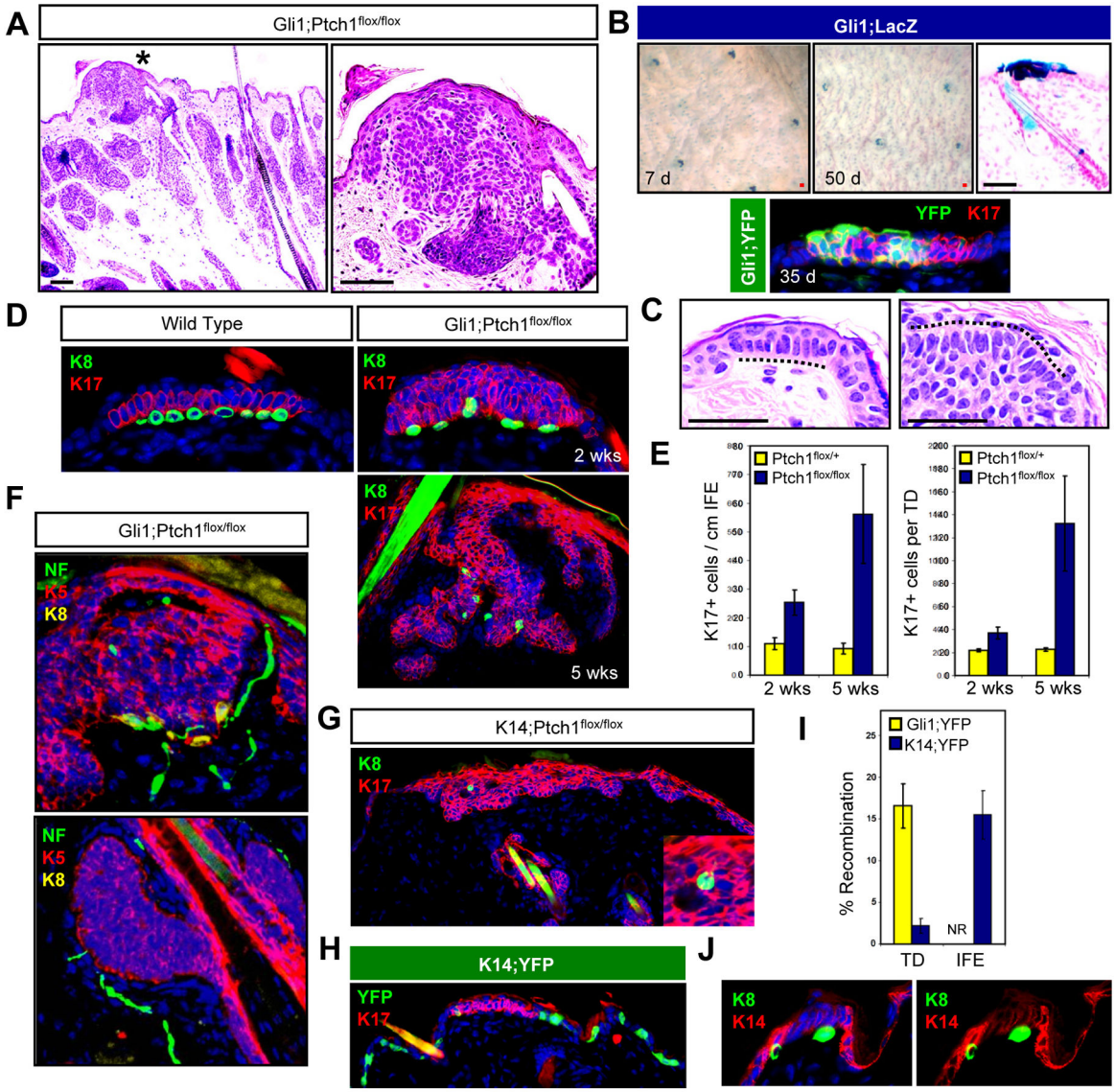

Figure 4. TDs are hot spots for tumor formation

A. H&E staining of a TD-associated lesion (*) in *Gli1;Ptch1* mice, 5 weeks post-TAM (left). Right, higher magnification view of (*). **B.** Top, whole mount LacZ staining of skin from *Gli1;LacZ* mice, 7 days (left) and 50 days (middle) post-TAM. Right, LacZ staining showing TD labeling. Bottom, IHC for YFP (green) and K17 (red) in a TD from a *Gli1;YFP* mouse, 35 days post-TAM. **C.** Resemblance of TD columnar basal cells with palisading periphery of a *Gli1;Ptch1* tumor (dotted lines). **D.** Top left, IHC of a normal TD, identified by K17 expression (red) and underlying K8+ Merkel cells (green). Right, tumorigenic TDs from *Gli1;Ptch1* mice, 2 and 5 weeks post-TAM. **E.** Quantitation of K17+ cells in the IFE and TD size in *Gli1;Ptch1* mice or controls, 2 and 5 weeks post-TAM. **F.** Top, TD-derived K5+ tumor (red) retaining underlying Merkel cells (yellow) associated with nerves, as identified by Neurofilament (NF, green). Bottom, hair follicle-associated tumors (red) with nerves in the dermis (green), but no Merkel cells. **G.** K8+ Merkel cells (arrow) are

associated with infrequent IFE-derived tumors, suggesting a TD origin. Inset, enlarged view. **H.** K14-Cre^{ERT} displays infrequent recombination in K17+ TD epithelia (red), and frequent recombination in the rest of the IFE, as assessed by YFP reporter expression (green). **I.** Quantitation of Gli1-Cre^{ERT2} and K14-Cre^{ERT} recombination rates in TD and non-TD IFE. NR, no recombination detected in non-TD IFE in *Gli1;YFP* mice. **J.** Reduced expression of K14 (red) in TDs overlying Merkel cells (green). Right panel is identical to the left, but with DAPI omitted. Data are represented as mean ± SEM. Scale bars, 50 μm.

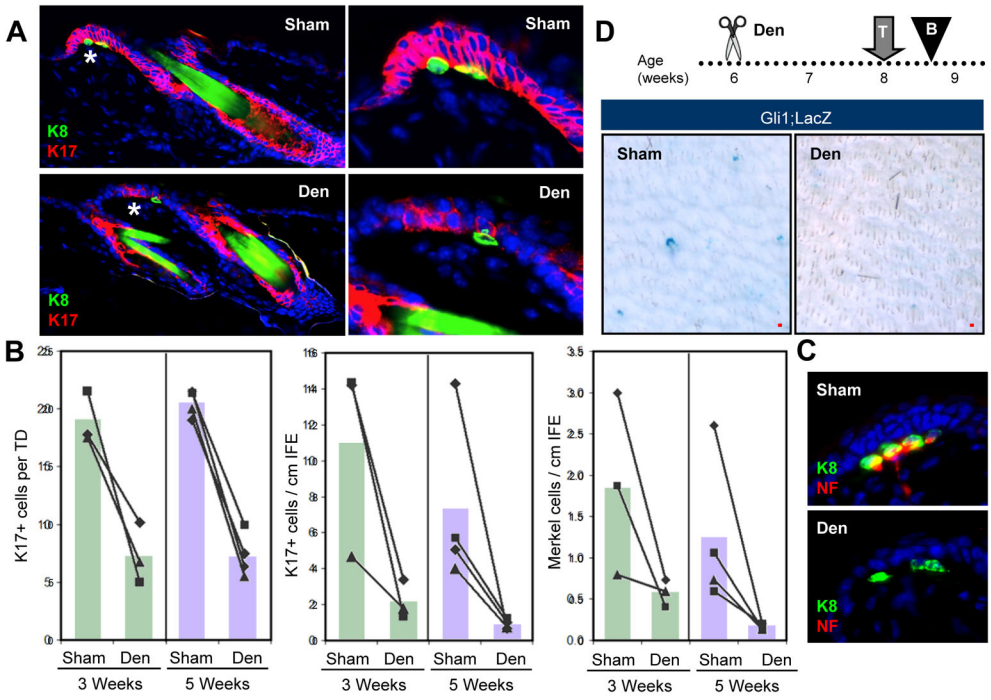

Figure 5. Innervation is required for Hh signaling in TDs

A. IHC of denervated ("Den") or sham-operated wild-type skin ("Sham") showing TD epithelia (red) and Merkel cells (green), 5 weeks after surgery. Right, magnified views of TD areas (*). **B.** Quantitation of the average size of K17+ TDs, as well as the overall abundance of K17+ cells and Merkel cells in the IFE, 3 and 5 weeks after denervation. Matched sham and denervated data from the same mice are connected by lines. **C.** Denervation causes stable loss of nerve endings (red) from Merkel cells (green), 3 weeks after surgery. **D.** Whole-mount LacZ staining showing that denervation inhibits induction of *LacZ* reporter expression in *Gli1;LacZ* mice. Den, denervation; T, TAM; B, biopsy. All superimposed bar graphs depict mean values. Scale bars, 50 μm. See also Figure S3.

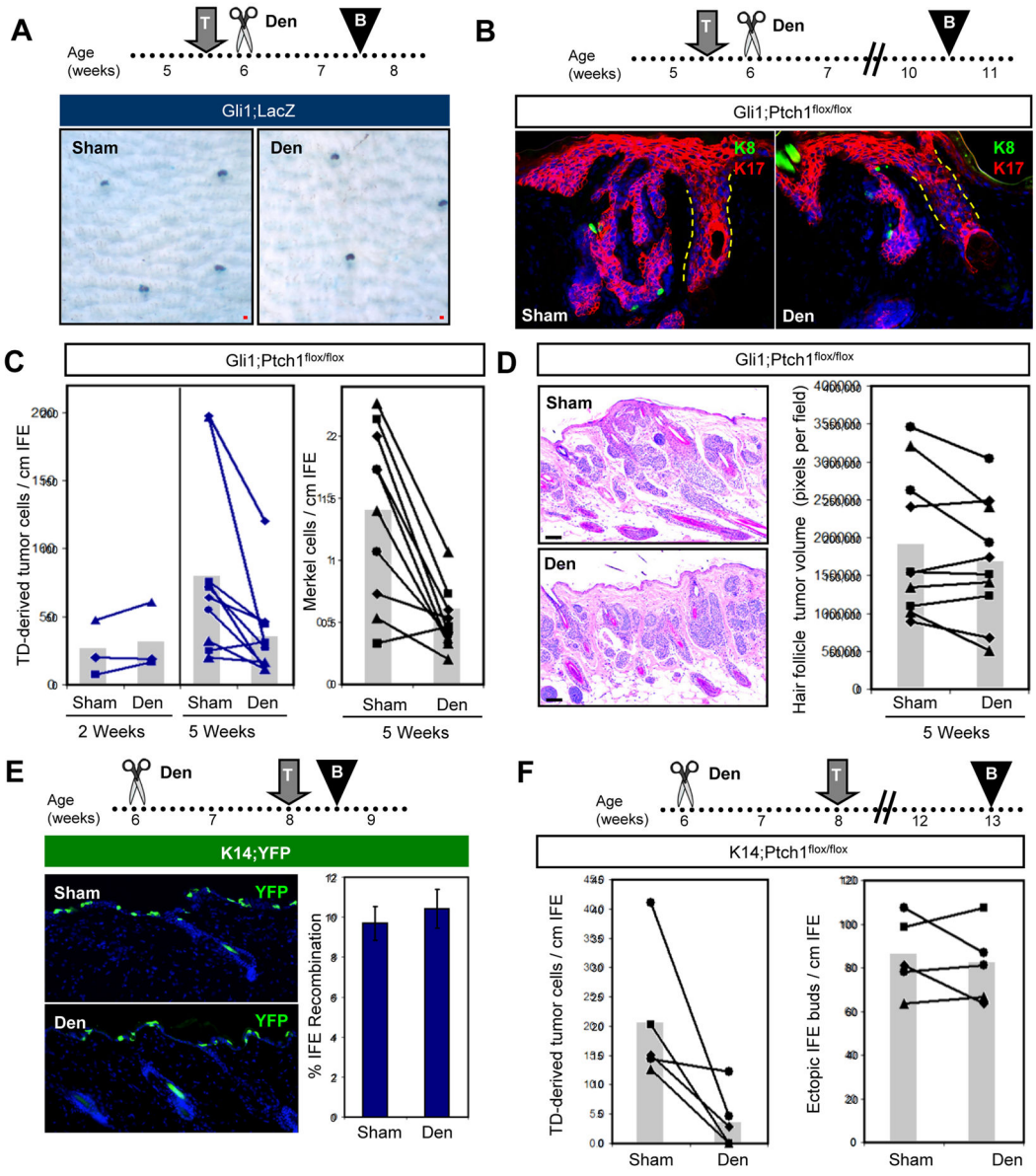

Figure 6. Denervation inhibits TD-derived tumors

A. Whole-mount LacZ staining of *Gli1;LacZ* skin, showing that denervation performed after TAM does not have an immediate effect on labeled *Gli1*-expressing TD cells (blue), 2 weeks after induction. **B.** IHC showing that denervation performed after TAM induction of *Gli1;Ptch1* mice reduces the size and complexity of TD-derived tumors (red). K8+ Merkel cells are labeled green (arrowheads). **C.** Quantitation of TD-derived tumor cells (left panel) and Merkel cell abundance (right panel), 2 and 5 weeks post-TAM. Matched sham and denervated data from the same mice are connected by lines. **D.** H&E and quantitation showing that denervation does not affect the abundance of hair follicle-derived tumors. **E.** IHC and quantitation showing that denervation does not affect K14-Cre^{ERT}-mediated recombination in the IFE. **F.** Quantitation showing that denervation inhibits tumor formation in TDs (left), but not the formation of ectopic IFE buds (right) in *K14;Ptch1* mice. Den,

denervation; T, TAM; B, biopsy. All superimposed bar graphs depict mean values. Data are represented as mean ± SEM. Scale bars, 50 μm. See also Figure S4.

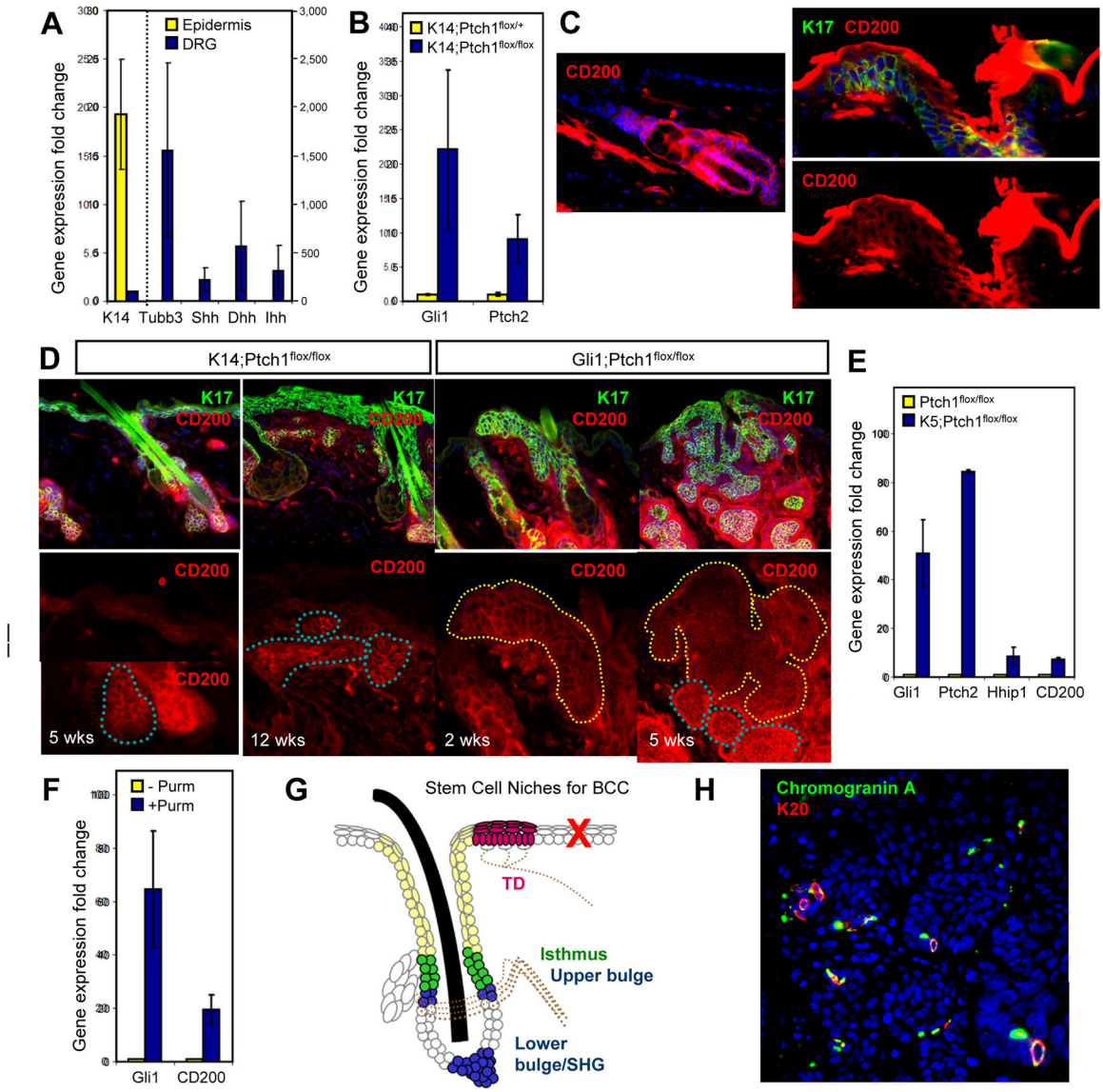

Figure 7. A mechanosensory niche promotes tumorigenesis

A. qPCR showing that DRG (blue bars) highly express all 3 Hh ligands (*Shh*, *Dhh*, *Ihh*) relative to epidermis (yellow bars). *K14* and *Tubulin ß3* (*Tubb3*) are specificity controls for skin and neurons, respectively. All values are expressed as fold induction relative to that of DRG (for *K14*, left y-axis) or epidermis (for all other genes, right y-axis). **B.** qPCR showing that *K14;Ptch1* mice, relative to non-tumorigenic controls, upregulate *Gli1* and *Ptch2* in the skin, 5 weeks post-TAM. **C.** IHC showing CD200 expression (red) throughout the hair follicle (left) and TD (right, dotted line), but not in the IFE. Top right, TD marked by K17 (green) and CD200, or CD200 alone (bottom right). **D.** Left panels, IHC showing that CD200 (red) is highly expressed in hair follicle-derived tumors (blue dotted lines), but weakly expressed in ectopic IFE buds or hyperplastic IFE (white dotted lines) in *K14;Ptch1* mice. Right panels, IHC showing that CD200 is highly expressed in TD-derived tumors (yellow dotted lines), both 2 and 5 weeks post-TAM, in *Gli1;Ptch1* mice. K17 (green) is

indiscriminately upregulated in hyperplastic IFE, ectopic IFE buds and tumors. All bottom panels are magnified views of the boxed areas. **E.** qPCR showing that keratinocytes harboring *K5* promoter-driven constitutive Cre and homozygous *Ptch1* flox alleles upregulate canonical Hh target genes as well as CD200. **F.** qPCR showing that the Smoothened agonist purmorphamine (purm) upregulates CD200 in wild-type keratinocytes. **G.** BCCs arise from multiple stem cell populations in the hair follicle and TD (filled regions). Tumors are also associated with the hair follicle infundibulum (beige), but do not arise efficiently from IFE stem cells (red 'X'). Tumors associated with the middle bulge region were not observed in this study, possibly due to inefficient Cre-mediated recombination in this domain. Dotted lines, nerves. SHG, secondary hair germ. **H.** IHC showing Merkel cells (arrowheads) expressing Chromogranin A (green) and K20 (red) in a human BCC. Inset is a magnified view of the region identified by the arrow. Data are represented as mean ± SEM. Scale bars, 50 μm. See also Figures S5–S7.